Influence of choice of small- and large-strain mode in FLAC on soil-geosynthetic interaction problems

Yan Yu
GeoEngineering Centre at Queen's-RMC, Royal Military College of Canada, Kingston, Ontario, Canada
Bo-Hung Lin
Department of Civil Engineering, National Chi Nan University, Taiwan
Richard J. Bathurst
GeoEngineering Centre at Queen's-RMC, Royal Military College of Canada, Kingston, Ontario, Canada

ABSTRACT
Soil-geosynthetic interaction plays a major role in the performance of mechanically stabilized earth structures such as reinforced soil walls, steep slopes and embankments. Program FLAC is now used routinely by engineers for the design and analysis of these structures. Accurate numerical modelling requires the use of appropriate constitutive models which has been the subject of much research. However, numerical outcomes may also be sensitive to geometric nonlinearity which is detectable when numerical simulations are carried out in both small- and large-strain modes in program FLAC. The paper examines two examples of soil-geosynthetic interaction problems using FLAC. The cases are: 1) horizontal pullout of a geosynthetic layer in a pullout box; and 2) a reinforced soil layer over a void. FLAC simulations are carried out both in small-strain mode (i.e., without numerical grid updating) and in large-strain mode (i.e., with numerical grid updating). Numerical results are used to quantitatively demonstrate good agreement between simulation results using the two modes for some cases and large differences in other cases. Examples of numerical results are demonstrated by comparing numerical outcomes using both approaches with physical test results available in the literature. This paper will assist engineers to identify those conditions where numerical simulations of geosynthetic-reinforced soil structures should be carried out in large-strain mode in order to avoid unreasonable numerical outcomes.

RÉSUMÉ
L'interaction sol-géosynthétiques joue un rôle majeur dans la performance des structures en sols stabilisés mécaniquement, telles que les murs, les pentes et les remblais renforcés. Le logiciel FLAC est maintenant utilisé de façon routinière pour le design et l'analyse de ces structures. La modélisation numérique précise requiert l'usage de modèles constitutifs appropriés qui ont été l'objet de beaucoup de recherche. Cependant, les résultats numériques peuvent aussi être sensibles à la non-linéarité géométrique qui est décelée lorsque les simulations numériques sont réalisées en modes faibles- et grandes- déformations du logiciel FLAC. L'article examine deux exemples de problèmes d'interaction sol-géosynthétiques en utilisant FLAC. Les cas sont : 1) l'arrachement horizontal d'une couche de géosynthétique dans une boîte d'arrachement; et 2) une couche de sol renforcé au-dessus d'une cavité. Les simulations FLAC sont réalisées en mode faibles-déformations (c.a.d. sans mise-à-jour de la grille numérique) et en mode grandes-déformations (c.a.d. avec mise-à-jour de la grille numérique). Les résultats numériques sont utilisés pour démontrer quantitativement le bon accord entre les résultats des simulations utilisant les deux modes pour quelques cas et les grandes différences dans d'autres cas. Des exemples de résultats numériques sont démontrés en comparant les résultats numériques obtenus par les deux approches, à des résultats d'essais physiques disponibles dans la littérature. Cet article aidera les ingénieurs à identifier les conditions pour lesquelles les simulations numériques des structures en sols renforcés de géosynthétiques devraient être réalisées en mode grandes-déformations pour éviter des résultats numériques déraisonnables.

1 INTRODUCTION

Geosynthetic-reinforced soil structures are widely accepted and used worldwide in civil, mining and coastal engineering applications. The internal stability design of routine (simple) structures is based on limit equilibrium "tied-back wedge" methods described in design guidelines such as CFEM (2006), AASHTO (2014) and BS8006 (2010). For more complex structures, numerical methods, such as the finite element method (FEM) and finite difference method (FDM) may be the only practical approaches to design a structure and/or to predict the deformation performance of these structures which cannot be carried out using force-based limit equilibrium methods.

Regardless of the general approach, calculations for internal stability analysis and design must include assumptions regarding geosynthetic-soil interaction between the horizontal sheets (or strips) of geosynthetic reinforcement that form the reinforced soil mass and are required to carry axial tensile load. Tensile load capacity is related to normal stresses acting on upper and lower sides of the reinforcement inclusions which are in vertical equilibrium (e.g., Abdelouhab 2011; Rowe and Skinner 2001; Damians et al. 2015; Yu et al. 2015a, b). However, the deformation of a geosynthetic-reinforced soil structure

during and at end of construction including surcharges applied to the soil backfill, can make the choice of interface model an important consideration when selecting details of the numerical solution approach. Other examples where considerations of this type are important are geosynthetic-reinforced soil layers located over potential voids such as sinkholes (e.g., Villard and Briancon 2008; Villard et al. 2009).

The objectives of this paper are to examine the influence of small- and large-mode options in the finite difference program FLAC (Itasca 2011) on the numerical outcomes of geosynthetic-reinforced soil structures and to identify the geosynthetic reinforcement loading conditions where the modelling of the soil-geosynthetic interaction should be carried out in the large-strain mode. Two examples are considered in this paper. The first example is a pullout test on a geogrid specimen placed horizontally and subjected to horizontal pullout loads under different applied normal pressures. The second example is a geotextile reinforced soil layer placed over a void subjected to unbalanced vertical stresses on upper and lower sides of the geotextile. Numerical outcomes from both examples are compared with physical test results available in the literature.

2 SMALL- AND LARGE-STRAIN MODE IN FLAC

The simulations in FLAC (Itasca 2011) can be carried out using either Lagrangian formulation (large-strain mode) or Eulerian formulation (small-strain mode). With Lagrangian formulation, the numerical grid coordinates are updated using the grid incremental displacements at each calculation step. The grid moves with the material to capture the deformed material geometry during modelling. Thus the stresses and displacements at each step are always based on the updated grid representing the deformed material zones (e.g., the geogrid inclusion and surrounding soil in the examples that follow).

When using Eulerian formulation, the numerical grid is fixed during modelling. The material zones move and deform, and the stresses and displacements at each step are calculated based on the initial defined grid. The deformed material zone geometry is not captured by the grid during modelling.

It should be noted that the constitutive stress-strain formulations in FLAC are based on the small-strain assumption for both Lagrangian and Eulerian formulations. However with very small incremental strains at each step, a large-strain formulation is approached by using many steps in FLAC large-strain mode with Lagrangian formulation (similar to a nonlinear curve fitted by many straight-line segments). More details regarding small- and large-strain mode options in FLAC can be found in the FLAC manual (Itasca 2011).

3 ILLUSTRATIVE EXAMPLES

This paper considers two examples related to geosynthetic-reinforced soil structures under different loading conditions: (a) geogrid pullout test where the horizontally placed geogrid layer is subjected to horizontal pullout loads (axial loading) and (b) geotextile over a void where the horizontally placed geotextile is loaded with unbalanced vertical stresses on upper and lower sides of the geotextile.

3.1 Example One: Geogrid Pullout Test

The geogrid pullout test in this paper is based on the physical test reported by Moraci and Recalcati (2006). Their pullout box was 1.70 m long, 0.60 m wide and 0.68 m high. The granular backfill soil had a maximum dry unit weight of γ_{dmax} = 16.2 kN/m^3 from Standard Proctor compaction tests. Direct shear tests (performed at 95% of γ_{dmax}) showed that the peak friction angle of the backfill soil was between ϕ_{ds} = 42° and 48°. A friction angle of ϕ_{ds} = 43° was deduced based on a best-fit straight line through four data points and forced through the origin of the shear strength versus applied vertical effective stress plot. The residual friction angle was ϕ_{cv} = 34°. The backfill was 0.6 m thick in the pullout box. The geogrid (GG3) modelled in this paper was the strongest of the three different extruded high density polyethylene (HDPE) mono-oriented geogrids tested by Moraci and Recalcati (2006). Geogrid GG3 had a tensile stiffness of $J_{2\%}$ = 1903 kN/m (tensile load at 2% axial strain) and ultimate tensile strength of T_f = 118 kN/m from the tensile tests performed at 1 mm/minute displacement rate. The modelled geogrid in this paper was 1.15 m long and 0.58 m wide and was tested under applied vertical effective pressures of σ_v = 10 and 50 kPa. The geogrid was located in the backfill at 0.3 m above the bottom of the pullout box.

Figure 1 shows the plane-strain FLAC numerical grid for the geogrid pullout test. The backfill was discretized into 3376 zones. The bottom of the backfill was fixed in *x*- and *y*-directions. Both left and right sides of the soil zone were fixed only in *x*-direction. In the original test, a 0.25 m-long sleeve surrounding the pullout clamp extended into the backfill. This arrangement was used to reduce the effect of the front pullout box boundary on the test results. Thus the soil boundaries above and below the sleeve were fixed in y-direction and the soil boundary at the end of the sleeve was fixed in *x*-direction (not shown in Figure 1).

The clamp located in the sleeve was initially extended into the soil (the clamp back end was at 0.35 m from the left soil boundary and no soil was present within the sleeve). The clamp was modelled by one beam element where both nodes were fixed in *x*- and *y*-directions. Three different pullout velocities were applied in the *x*-direction (i.e., 1×10^{-6}, 1×10^{-7}, and 5×10^{-8} m/step) for both nodes of the beam element. It should be noted that these pullout velocities are related to numerical steps in FLAC static analysis and cannot be equated to actual pullout velocities. Geogrid pullout loads in the physical tests (Moraci and Recalcati (2006) were calculated by subtracting the sleeve friction load (which was measured from a separate test with the sleeve only) from the measured clamp load at the same displacement. Thus the interaction between the clamp and backfill was not modelled in the current study. The geogrid was modelled using cable elements with a total of 115 elements. The

first cable node (at geogrid front end) was slaved to the second beam node (at clamp back end) to keep these two nodes locked together with the same *x*- and *y*-displacements. The numerical modelling was repeated using small- and large-strain modes.

The soil was modelled as a linear elastic-plastic material (i.e., Mohr-Coulomb model). The soil was assigned a unit weight of γ_b = 95%×γ_{dmax} = 0.95×16.2 = 15.4 kN/m^3 and a plane-strain friction angle of ϕ_{ps} = tan^{-1} (1.2×ϕ_{ds}) = tan^{-1}(1.2×43°) = 48°. The soil dilation angle was taken as ψ_b = 18°. The soil apparent cohesion was set to c_b = 1 kPa. The Young's modulus of the backfill was 30 MPa and the Poisson's ratio was 0.3. The clamp properties were not important and did not affect the numerical results because the two beam nodes move with the same velocity in x-direction which results in zero axial load within the beam. The geogrid pullout loads (with unit of kN/m) reported by Moraci and Recalcati (2006) were calculated from the measured pullout forces (with unit of kN) divided by the geogrid width of 0.58 m. Thus the geogrid (modelled by cable elements) was simulated with an out-of-plane width of 1 m. The cable elements had a cross-sectional area of A_g = 0.002 m^2 and perimeter of P_g = 2 m based on the assumed thickness of 2 mm (this assumed geogrid thickness did not affect numerical results). The Young's modulus of the cable elements was E_r = $J_{2\%}/A_r$ = 1903/0.002 = 9.515×10^5 kPa. A strength reduction factor of R_i = 0.67 was applied to the soil-geosynthetic interface resulting in a friction angle of the cable grout of ϕ_{sg} = tan^{-1}(Ri×tan(ϕ_{ps})) = tan^{-1}(0.67×tan(48°)) = 36.7° and cohesive strength component of C_{sg} = R_i×c×P_g = 0.67×1×2 = 1.34 kN/m. The shear stiffness of the grout was set to $K_{s,sg}$ = 20 MN/m/m. The tensile yield strength of the cable element was taken to be same as the geogrid ultimate tensile strength (i.e., 118 kN/m). More detailed information on the calculation of cable properties can be found in the paper by Yu et al. (2015a).

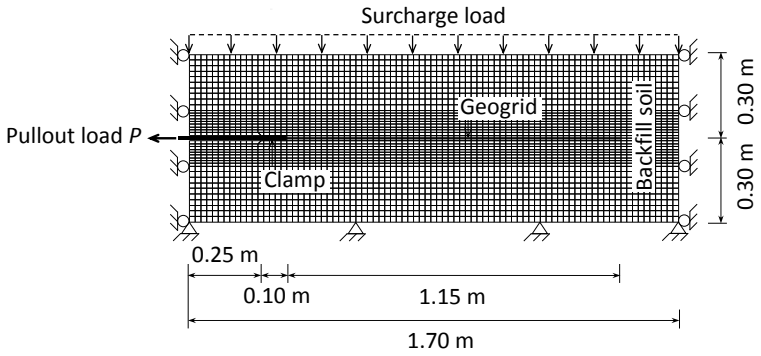

Figure 1. Pullout test model showing horizontal geogrid subjected to horizontal pullout load, FLAC numerical grid and boundary conditions.

The calculated pullout load curves at three different pullout velocities using FLAC in small-strain mode are shown in Figure 2. Decreasing the pullout velocity from 1×10^{-6} to 5×10^{-8} m/step decreased the calculated pullout loads when other conditions were equal. The lowest pullout velocity resulted in less unbalanced force in the numerical model and thus more accurate results when using FLAC for static analysis. The differences in pullout loads for pullout velocities of 1×10^{-7} and 5×10^{-8} m/step were minor. The predicted peak pullout load for the test at vertical effective stress of 10 kPa and pullout velocity of 1×10^{-6} agreed well with the measured peak pullout load but the numerical simulation overestimated the residual pullout load. The numerical pullout curves for the same test but at pullout velocities of 1×10^{-7} and 5×10^{-8} m/step slightly underestimated the peak pullout load but were in agreement with the measured residual pullout load. At the applied vertical effective stress of 50 kPa, the predicted pullout load-displacement responses using all three pullout velocities were in good agreement at geogrid displacements less than 15 mm, but overestimated the pullout loads at larger displacements.

Figure 3 shows the predicted pullout load-displacement curves at three different pullout velocities using FLAC in large-strain mode. Observations made for Figure 2 also apply here with the exception that the load-displacement responses at the two highest velocities and a vertical effective stress of 50 kPa are in better agreement with measured data at large displacements. Figure 4 shows results of numerical tests carried out with pullout velocity of 5×10^{-8} m/step and in small- and large-strain mode. Pullout loads were consistently lower at post-peak pullout load for simulations carried out in large-strain mode.

However, from a practical point of view, the influence of small- and large-strain mode on pullout load response is judged to be negligible for the geogrid pullout tests and boundary conditions examined in this paper.

The predicted geogrid strains from numerical tests carried out at pullout velocity of 5×10^{-8} m/step are shown in Figure 5. The results indicate that the influence of small- and large-strain mode on geogrid axial strains was negligible. Figure 5 also shows that the geogrid strains using FLAC in large-strain mode (and 50 kPa vertical effective stress) extend over a longer distance than those in the matching small-strain mode simulation (the initial geogrid length was 1.15 m). This is visual evidence of numerical grid and structure geometry updating that occurs when FLAC is run in large-strain mode.

In summary, the selection of small- or large-strain mode in FLAC had minor quantitative influence on pullout load-displacement behaviour and geogrid axial strains for the geogrid pullout test examined in this paper. This was because the geogrid reinforcement was arranged horizontally and subjected to horizontal (axial) pullout loads with balanced vertical stresses acting on the upper and lower sides of the geogrid inclusion.

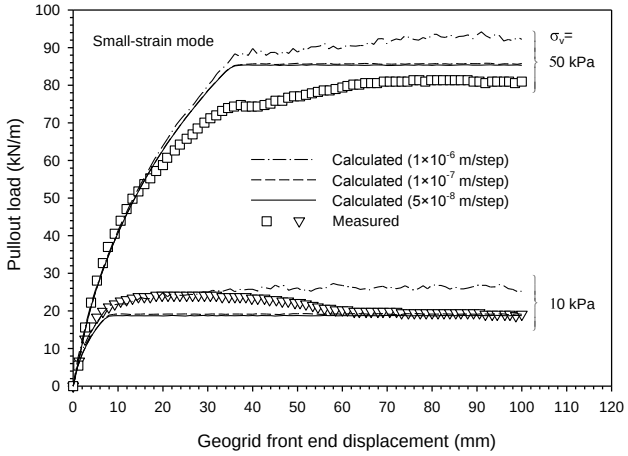

Figure 2. Measured and predicted pullout load curves using FLAC in small-strain mode.

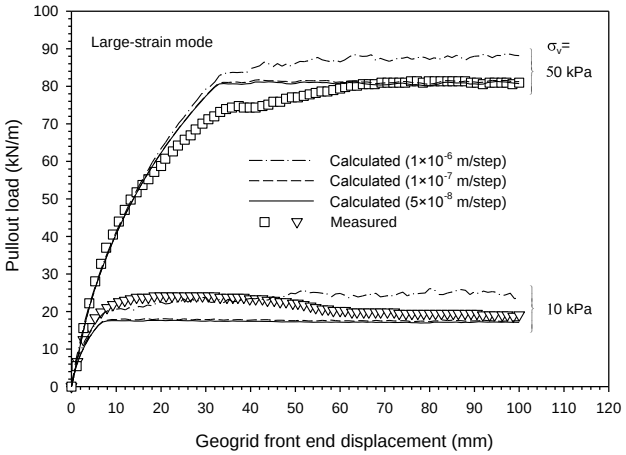

Figure 3. Measured and predicted pullout load curves using FLAC in large-strain mode.

3.2 Example Two: Geotextile Over A Void

Villard and Briancon (2008) reported the results of a test with a geotextile reinforcement layer located below a layer of soil and placed over a void. The test was carried out in a shallow trench with a cavity formed in the trench. The cavity was initially supported by two inflated air bags. A geotextile (tensile stiffness of J = 1100 kN/m in the longitudinal direction and tensile rupture strength of T_f = 125 kN/m measured at 12% of strain) was placed at the bottom of the trench over the air bags. Next, the trench was backfilled with a gravel layer with thickness h_g = 0.5 m and compacted to unit weight of γ_g = 17.0 kN/m^3. The Young's modulus of the supporting soil (original ground) was E_s = 30 MPa. Other properties of the gravel layer and supporting soil were not reported. The interface between the gravel and geotextile had a friction angle of ϕ_{upper} = 30° and the interface friction angle between the supporting soil and geotextile was ϕ_{lower} = 25°. The physical test was carried out by deflating air bags and removing the two air bags to ensure that there was no support for the geotextile over the resulting void. The reinforced soil layer was subsequently surcharged but this stage of the physical test program is not simulated in the current study.

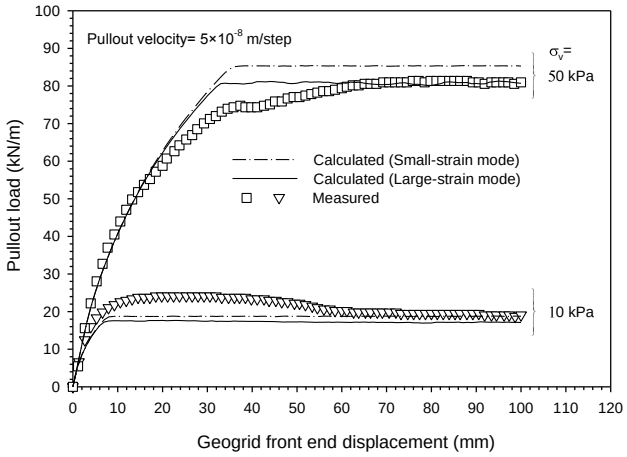

Figure 4. Influence of small- and large-strain mode in FLAC on predicted pullout load-displacement response.

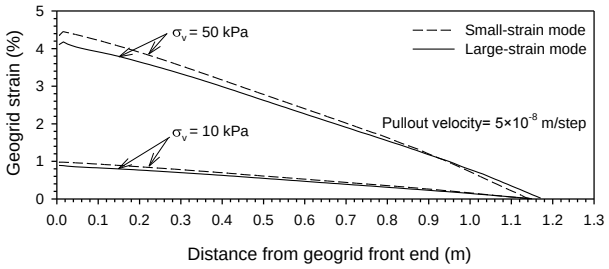

Figure 5. Influence of small- and large-strain mode in FLAC on predicted geogrid axial strains.

Numerical modelling of the geotextile-reinforced soil layer over the void was performed using FLAC with two different methods as shown in Figure 6. The physical test was performed under the plane-strain conditions and thus an out-of-plane width of 1 m was modelled. The model in-plane horizontal length was 10 m (starting from the left fixed end of the geotextile). The simplified method (Figure 6a) only simulates the deformations of the geotextile and the supporting soil below the geotextile was considered to be rigid. To generate an interface between the supporting soil and geotextile, a total of 200 0.1-m thick zones was initially generated with all nodes fixed in x- and y-directions. The gravel layer above the geotextile was simplified as a uniform surcharge load ($q = \gamma_d h_g$ = 17×0.5

= 8.5 kPa) acting on the geotextile without considering the interaction between the gravel layer and geotextile (e.g., no shear stresses acting on the upper side of the geotextile). This method is similar to that used by Villard and Briancon (2008) in their FEM model. The soil-geosynthetic interaction method (Figure 6b) modelled the geotextile, the gravel layer above the geotextile and the supporting soil below the geotextile. Hence, geotextile deformations were influenced by the properties of and interactions between the geotextile, gravel layer and supporting soil. The supporting soil had a Young's modulus of 30 MPa and relatively high apparent cohesive strength and thus only a 0.5 m-thick layer of supporting soil was required in the model. Increasing the thickness of the supporting soil had minor effect on the numerical results reported in this investigation. The gravel layer and support soil were discretized into 2000 zones. The bottom of the supporting soil was fixed in *x*- and *y*-directions. The left and right sides of the modelled region were fixed in *x*-direction only. Two interfaces were generated to model the soil-geosynthetic interaction (one between the gravel layer and geotextile, and the other between the supporting soil and geotextile). The geotextile was modelled using beam elements in FLAC with a total of 200 elements for both simplified and soil-geosynthetic interaction methods. The left end of the geotextile was fixed in *x*- and *y*-directions and the right end was free.

Both the gravel layer and supporting soil were taken as Mohr-Coulomb materials. The friction angle of the gravel was set to $\phi_g = 44°$ as reported by Villard et al. (2009) for the same test site. Thus the interface reduction factor was calculated to be $R_i = \tan(\phi_{upper})/\tan(\phi_g) = \tan(30°)/\tan(44°) = 0.6$. Based on this interface reduction factor, the friction angle of the supporting soil was set to $\phi_s = \tan^{-1}(\tan(\phi_{lower})/R_i) = \tan^{-1}(\tan(25°)/0.6) = 38°$. The dilation angles of the gravel and supporting soil were taken to be $\psi_g = 14°$ and $\psi_s = 8°$, respectively. The apparent cohesion of the gravel was set to $c_g = 1$ kPa and the supporting soil was assumed to have an apparent cohesion of $c_s = 10$ kPa because failure of the supporting soil at the left and right sides of the void was not observed during the physical test. The unit weight of the supporting soil was set to $\gamma_s = 16.0$ kN/m^3. The Young's modulus of the gravel was taken to be $E_g = 40$ MPa. The interfaces above and below the geotextile were assumed to be non-dilatant ($\psi_{upper} = \psi_{lower} = 0$). The interface cohesion between the gravel layer and geotextile was taken to be $c_{upper} = R_i \times c_g = 0.6 \times 1 = 0.6$ kPa. For the interface between the supporting soil and geotextile, the cohesion was $c_{lower} = R_i \times c_s = 0.6 \times 10 = 6$ kPa. Both interfaces had a normal stiffness of $k_n = 1000$ MPa and a shear stiffness of $k_s = 10$ MPa. The geotextile (modelled by beam elements) was simulated with an out-of-plane width of 1 m (plane-strain condition). The beam elements had a cross-sectional area of $A_g = 0.002$ m^2 and perimeter of $P_g = 2$ m where the thickness of the geotextile was assumed to be 2 mm. The geotextile thickness had no influence on the numerical results. It is the geotextile stiffness that influences numerical results. The Young's modulus of the beam elements was $E_r = J/A_r = 1100/0.002 = 5.5 \times 10^5$ kPa. The geotextile and lower interface properties for the simplified method were the same as those for the soil-geosynthetic interaction method. For the simplified method with uniform load applied directly to the beam elements (Figure 6a), a small moment of inertia ($I = 1 \times 10^{-8}$ m^4) for the beam elements was required to successfully transfer the uniform surcharge loads to the beam elements. This small beam element moment of inertia had minor effect on the geotextile deformation and axial loads. For the soil-geosynthetic interaction method (Figure 6b) the moment of inertia for the beam elements was $I = 0$. The model (including zones in the void) was initially solved to reach force equilibrium; thereafter the zones in the void were removed and the model was solved to final force equilibrium.

Figure 7 shows the calculated displacement vectors using the simplified method defined in Figure 6a. When FLAC was executed in small-strain mode, the model failed to converge after removing the zones in the void and the maximum calculated vertical displacement of the geotextile was about 1.80 m only after 2000 steps (Figure 7a). It should be noted that the maximum measured vertical displacement of the geotextile in the physical experiment was about 0.23 m (Villard and Briancon 2008). When using FLAC in large-strain mode, final force equilibrium was reached after removing the zones in the void and the maximum calculated vertical displacement of the geotextile was about 0.23 m which agrees well with the measured value of 0.23 m.

The calculated displacement vectors with the soil-geosynthetic interaction method (defined in Figure 6b) are shown in Figure 8. For the FLAC simulation using small-strain mode, the model did not achieve force equilibrium after removing the zones in the void. The maximum calculated vertical displacement of the geotextile was about 1.26 m after 10000 steps. Using FLAC in large-strain mode resulted in force equilibrium and a maximum calculated vertical displacement of 0.21 m for the geotextile. This value is in good agreement with the physical test result of 0.23 m reported earlier.

Figure 9 shows the measured and calculated geotextile strains after removing the air bags to create the underlying void. The numerical results show that the calculated geotextile strains using FLAC with the simplified method agree well with those calculated by Villard and Briancon (2008) who used a FEM model with the simplified method. The calculated maximum geotextile strains were located at the left and right edges of the void for both FLAC and FEM simulations and the simplified method. Using FLAC with the soil-geosynthetic interaction method, the calculated maximum geotextile strain occurred above the middle of the void (i.e., at 3 m from geotextile left end in Figure 9). The calculated strains using FLAC with the soil-geosynthetic interaction method agreed well with the physical data measured shortly after removing the supporting air bags. Due to the time-dependent stiffness of the geosynthetic material, the geotextile strains were larger when measured 5 months later. The time-dependent behaviour of the geotextile was not attempted in this study since load-strain-time data were not available for the geotextile. Strategies to model the load-strain-time behaviour of geosynthetic reinforcement materials can be found in the literature

(e.g., Walters et al. 2002; Allen and Bathurst 2014; Ezzein et al. 2015).

In summary, numerical modelling of a geotextile-reinforced soil layer over a void showed that using the small-strain mode in FLAC (without updating the soil and structure geometry) was not able to reach the force equilibrium when part of the geotextile was unsupported by the underlying soil. This was because the horizontal geotextile could not support unbalanced vertical stresses on the upper and lower sides of the geotextile when using the small-strain mode in FLAC. Stated alternatively, the horizontal structure elements can only generate horizontal axial loads and these horizontal loads cannot balance the vertical loads acting on the horizontal structure elements. However, using the large-strain mode in FLAC resulted in force equilibrium and good agreement between measured and calculated geotextile deformations and strains.

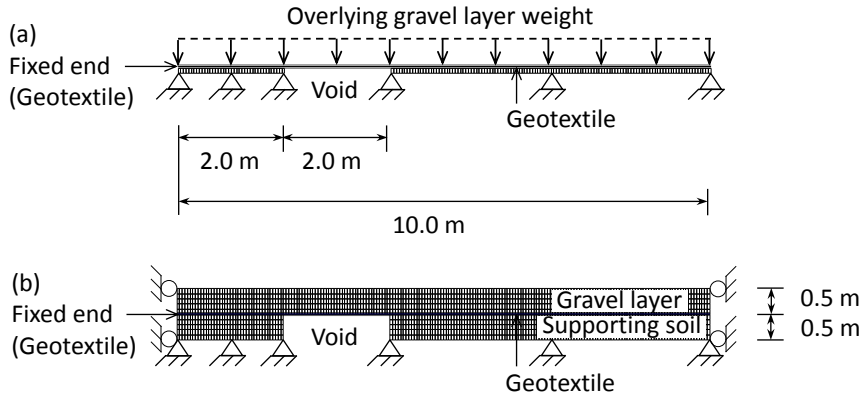

Figure 6. Reinforced geotextile layer over void subjected to unbalanced vertical stresses on upper and lower sides of the geotextile using FLAC with (a) simplified method (all numerical grid nodes are fixed in *x*- and *y*-direction) and (b) soil-geosynthetic interaction method.

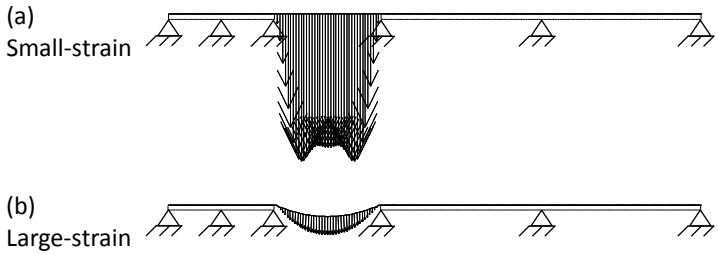

Figure 7. Calculated displacement vectors using FLAC with simplified method: (a) small-strain mode without reaching final force equilibrium (the maximum vertical displacement of the geotextile is about 1.80 m after 2000 steps) and (b) large-strain mode after reaching final force equilibrium (the maximum vertical displacement of the geotextile is about 0.23 m).

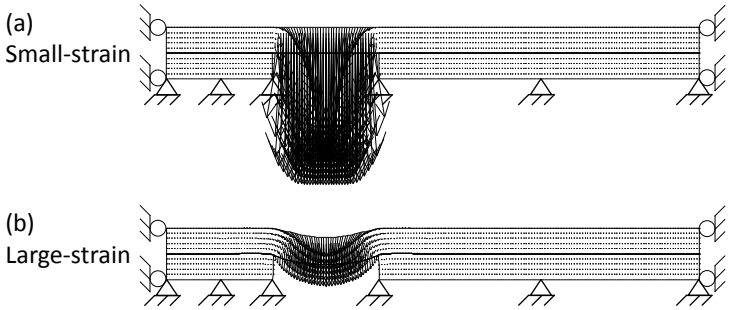

Figure 8. Calculated displacement vectors using FLAC with soil-geosynthetic interaction method: (a) small-strain mode without reaching final force equilibrium (the maximum vertical displacement of the geotextile is about 1.26 m after 10000 steps) and (b) large-strain mode after reaching final force equilibrium (the maximum vertical displacement of the geotextile is about 0.21 m).

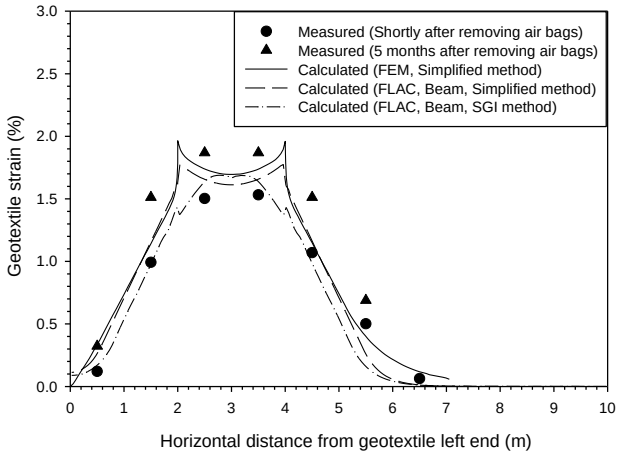

Figure 9. Measured and calculated geotextile strains after removing the air bags to create underlying void. Note: SGI = soil-geosynthetic interaction.

4 CONCLUSIONS

Numerical modelling of geosynthetic-reinforced soil walls and geosynthetic-reinforced layers over voids are two examples where FEM and FDM techniques are attractive numerical modelling approaches. However, the accuracy of numerical models using program FLAC depends not only on the soil and geosynthetic constitutive models, but also on the choice of small-strain mode (i.e., without updating soil and structure geometry during calculations) and large-strain mode (i.e., updating soil and structure geometry). This paper reports the results of simulations of two cases related to geosynthetic-reinforced soil structures using FLAC with both small- and large-strain modes activated: (a) geogrid pullout test, and (b) geotextile-reinforced soil layer over a void.

The numerical modelling results for the geogrid pullout test showed that the pullout loads using the small-strain mode in FLAC were larger than those using the large-strain mode when other conditions were the same. However, the influence of small- and large-strain mode on the calculated pullout loads was minor and judged to be negligible from a practical point of view. The calculated pullout loads from both small- and large-strain modes (with pullout velocity higher than 1×10^{-7} m/step) generally agreed with measured values. The numerical analyses also indicated that the response of the horizontally placed geosynthetic sheet when subjected to horizontal axial pullout loads can be modelled sufficiently accurately using either the small-strain or large-strain mode option in FLAC.

The modelling of a geotextile-reinforced soil layer over a void showed that the FLAC code in small-strain mode failed to converge. However, the program was able to reach force equilibrium when used in large-strain mode. The calculated maximum geotextile vertical displacement and geotextile strains from simulations with large-strain mode in FLAC generally agreed well with the measured data. The modelling results indicate that a horizontal geosynthetic sheet subjected to unbalanced vertical stresses between the upper and lower sides of the geosynthetic sheet should be modelled using large-strain mode in FLAC to avoid unreasonable numerical outcomes.

ACKNOWLEDGEMENTS

The work reported in this paper was supported by grants from the Natural Sciences and Engineering Research Council of Canada (NSERC) and the Graduate Students Study Abroad Program of the National Science Council, Republic of China (Taiwan).

REFERENCES

Abdelouhab, A., Dias, D., and Freitag N. 2011. Numerical analysis of the behaviour of mechanically stabilized earth walls reinforced with different types of strips. *Geotextiles and Geomembranes*, 29: 116-129.

American Association of State Highway and Transportation Officials (AASHTO), 2014. *LRFD bridge design specifications*, 7th Edition, Washington, DC.

Allen, T.M., and Bathurst, R.J. 2014. Performance of an 11 m high block-faced geogrid wall designed using the K-stiffness method. *Canadian Geotechnical Journal*, 51(1): 16-29.

Bathurst, R.J., and Kaliakin, V.N. 2005. Review of numerical models for geosynthetics in reinforcement applications. *In Proceedings of the 11th International Conference on Computer Methods and Advances in Geomechanics*, Torino, Italy, Vol. 4, pp. 407-416.

BS8006, 2010. *Code of Practice for Strengthened/ Reinforced Soil and Other Fills*, British Standards Institution (BSI). Milton Keynes, UK.

CFEM, 2006. *Canadian Foundation Engineering Manual*, 4th Edition. BiTech Publishers, Richmond, BC

Damians, I.P., Bathurst, R.J., Josa, A., and Lloret, A. 2015. Numerical analysis of an instrumented steel reinforced soil wall. *International Journal of Geomechanics ASCE*, 15(1), 04014037.

Ezzein, F., Bathurst, R.J., and Kongkitkul, W. 2015. Non-linear load-strain modelling of polypropylene geogrids during constant rate-of-strain loading. *Polymer Engineering and Science,* doi: 10.1002/pen.23999.

Itasca. 2011. FLAC: *Fast Lagrangian Analysis of Continua*. Version 7.0 [computer program]. Itasca Consulting Group, Inc., Minneapolis, Minn.

Moraci, N., and Recalcati, P. 2006. Factors affecting the pullout behavior of extruded geogrids embedded in a compacted granular soil. *Geotextiles and Geomembranes*, 24: 220-242.

Rowe, R.K., and Skinner, G.D. 2001. Numerical analysis of geosynthetic reinforced retaining wall constructed on a layered soil foundation. *Geotextiles and Geomembranes*, 19: 387-412.

Villard, P., and Briancon, L. 2008. Design of geosynthetic reinforcements for platforms subjected to localized sinkholes. *Canadian Geotechnical Journal*, 45: 196-209.

Villard, P., Chevalier, B., Le Hello, B., and Combe, G. 2009. Coupling between finite and discrete element methods for the modelling of earth structures reinforced by geosynthetic. *Computers and Geotechnics,* 36: 709-717.

Walters, D.L., Allen, T.M., and Bathurst, R.J. 2002. Conversion of Geosynthetic Strain to Load using Reinforcement Stiffness. *Geosynthetics International*, 9(5-6): 483-523.

Yu, Y., Damians, I.P., and Bathurst, R.J. 2015a. Influence of choice of FLAC and PLAXIS interface models on reinforced soil-structure interactions. *Computers and Geotechnics*, 65: 164-174.

Yu, Y., Bathurst, R.J., and Miyata, Y. 2015b. Numerical analysis of a mechanically stabilized earth wall reinforced with steel strips. *Soils and Foundations,* 55, doi:10.1016/j.sandf.2015.04.006.